Structural Engineering and Mechanics, Vol. 45, No.4 (2013) 543-568
DOI: http://dx.doi.org/10.12989/sem.2013.45.4.543

AGV-induced floor micro-vibration assessment in LCD factories by using a regressional modified Kanai-Tajimi moving force model

C.L. Lee[1a], R.K.L. Su[*1] and Y.P. Wang[2b]

[1]*Department of Civil Engineering, The University of Hong Kong, Hong Kong, China*
[2]*Department of Civil Engineering, National Chiao-Tung University, Hsinchu, Taiwan*

(Received March 28, 2011, Revised November 26, 2012, Accepted January 21, 2013)

Abstract. This study explores the floor micro-vibrations induced by the automated guided vehicles (AGVs) in liquid-crystal-display (LCD) factories. The relationships between moving loads and both the vehicle weights and speeds were constructed by a modified Kanai-Tajimi (MKT) power spectral density (PSD) function whose best-fitting parameters were obtained through a regression analysis by using experimental acceleration responses of a small-scale three-span continuous beam model obtained in the laboratory. The AGV induced floor micro-vibrations under various AGV weights and speeds were then assessed by the proposed regressional MKT model. Simulation results indicate that the maximum floor micro-vibrations of the target LCD factory fall within the VC-B and VC-C levels when AGV moves at a lower speed of 1.0 m/s, while they may exceed the acceptable VC-B level when AGV moves at a higher speed of 1.5 m/s. The simulated floor micro-vibration levels are comparable to those of typical LCD factories induced by AGVs moving normally at a speed between 1.0 m/s and 2.0 m/s. Therefore, the numerical algorithm that integrates a simplified sub-structural multi-span continuous beam model and a proposed regressional MKT moving force model can provide a satisfactory prediction of AGV-induced floor micro-vibrations in LCD factories, if proper parameters of the MKT moving force model are adopted.

Keywords: micro-vibration; automated guided vehicle (AGV); liquid-crystal-display (LCD); moving loads; modified Kanai-Tajimi model; power spectral density (PSD)

1. Introduction

The development of thin-film-transistor liquid-crystal-display (TFT-LCD) (Jang and Choi 2006) has become one of the fastest growing industries in the past decade, especially in Korea, Japan, China, and Taiwan, due to the strong market demand for products such as displays for computers, mobile telephones, digital cameras, and flat-screen televisions. The TFT-LCD industry specialises in glass panels as opposed to silicon wafer, which is used in the semiconductor industry, but adopts similar micro-vibration criteria, fabrication processes, and equipment. The manufacturing

∗Corresponding author, Associate Professor, E-mail: klsu@hkucc.hku.hk
[a]Former postdoctoral Fellow
[b]Professor

Fig. 1 Automated guided vehicles used in LCD factories (http://www.muratec.net/mac/products/fpd/agv.html)

processes of silicon wafers and glass panels are susceptible to a variety of vibration sources. Significant interior vibration sources include pumps, motors, carts, servo robots, conveying systems, personnel walking (Nguyen *et al*. 2012), and automated material handling systems (AMHS, Jang and Choi 2006). Exterior ground-borne sources may include supply mechanical equipment in neighbouring buildings, nearby traffic, rail lines (high-speed trains), and pile construction. If the ambient floor vibration does not meet the vibration criteria, a satisfactory production yield of the chips or displays will not be achieved. The BBN (Bolt, Beranek, and Newman) vibration criterion (VC) is one of the most popular criteria used for vibration-sensitive equipment in high-tech industry (Gordon 1991). The VC curves are a set of one-third octave band velocity spectra labeled as VC-A, VC-B, VC-C, VC-D, and VC-E (Fig. 2) that correspond to the allowable root-mean-square (RMS) velocity from 2000 μ-inch/s to 125 μ-inch/s within a frequency ranging from 8 Hz to 100 Hz. For frequencies below 8 Hz, the VC curves allow for greater vibration velocity because this frequency range lies below the lowest natural (resonance) frequency of most of the equipment, as indicated by Gordon (1991). Normally, the VC-B (1000 μ-inch/s) or VC-C (500 μ-inch/s) levels are acceptable for most vibration-sensitive tools, as required by the LCD manufacturers (Tang *et al*. 2009).

Over the last two decades, micro-vibrations have been extensively studied in the context of human comfort and production yield for office buildings, biotechnology or metrology labs, and semiconductor factories (Ungar and White 1979, Pavic and Reynolds 2002, Ungar *et al*. 2004, Pavic and Reynolds 2003, Willford *et al*. 2005, Pan *et al*. 2008, Živanović and Pavić 2009, Pan *et al*. 2001, Xu and Hong 2008, Ju 2009, Yang and Agrawal 2000, Xu *et al*. 2004, Xu and Guo 2006). Most of the studies presented in the literature focused on the floor vibrations induced by exterior ground-borne traffic (train) excitations or from the personnel walking and mechanical disturbance sources inside the building. However, those adverse vibrations that are directly induced by moving vehicles on the production floor in high technology fabrication facilities (or called 'fab') have rarely been considered in the design phase. Currently, the transportation of glass panels between processing tools in LCD factories is generally accomplished by automated guided vehicles (AGVs shown in Fig. 1), rail guided vehicles (RGVs), and stockers (Jang and Choi, 2006). As a consequence, most of the LCD factories encounter interior vehicle-induced floor micro-vibration problems when they begin operations. Fig. 2 shows typical AGV- or stocker-

induced floor micro-vibration spectra measured by the authors in several LCD factories, in which "RC Floor" and "Foundation" are used to represent the vibrations measured on the RC floors and on the top surfaces of the foundations that support precision tools, respectively. The micro-vibration in the vertical direction (Z) is shown to be more pronounced than those in the horizontal directions (X and Y), and the peak floor micro-vibration may reach the VC-B level or even exceed the VC-A level, depending on the AGV weight and moving speed. The AGVs, RGVs, and stockers have been found to induce considerably more significant floor micro-vibrations than personnel walking or nearby traffic, and this has become more serious in the LCD industry as increasingly larger glass panels are being manufactured.

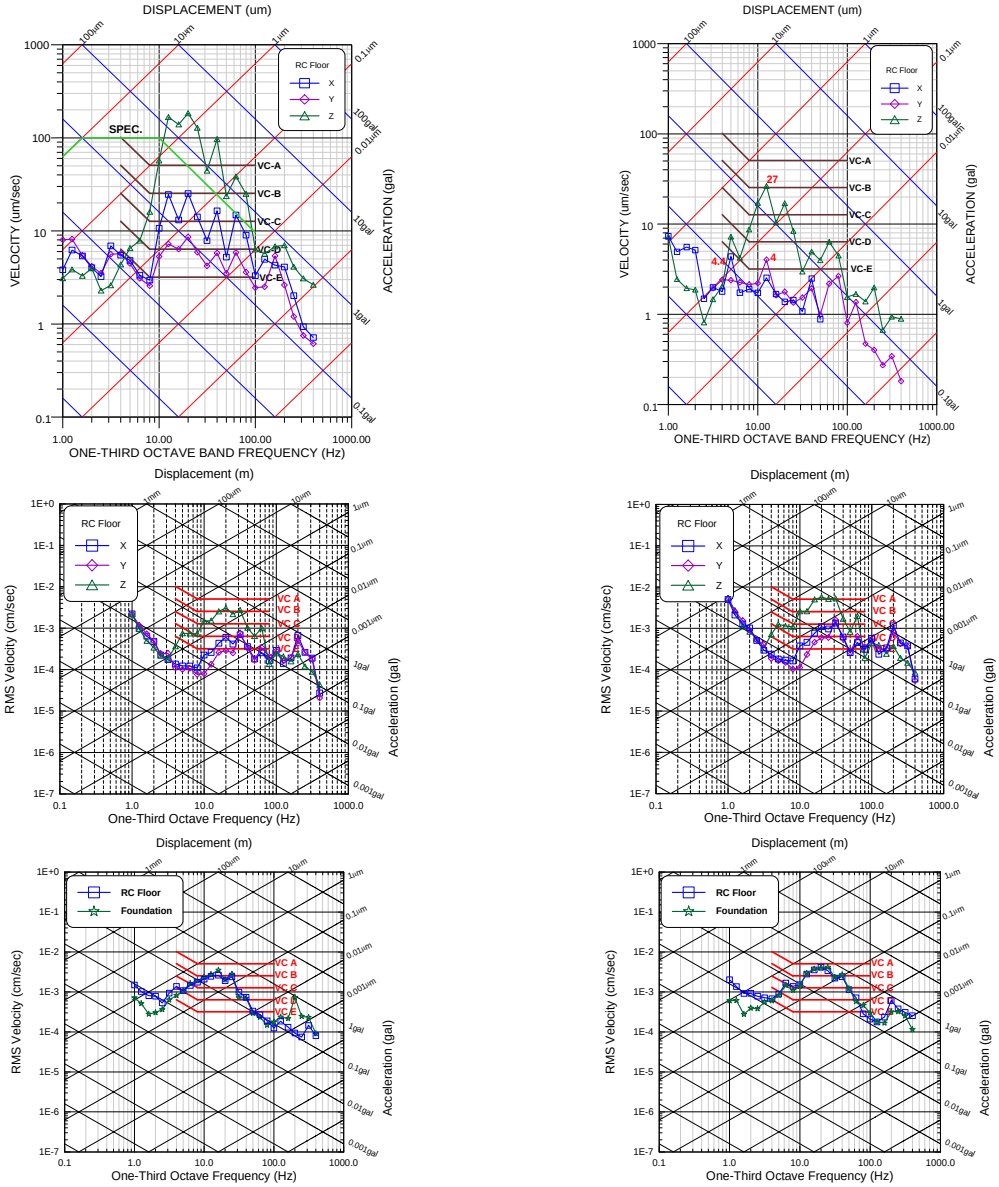

Fig. 2 Measured AGV- or stocker-induced micro-vibration spectra in typical LCD factories

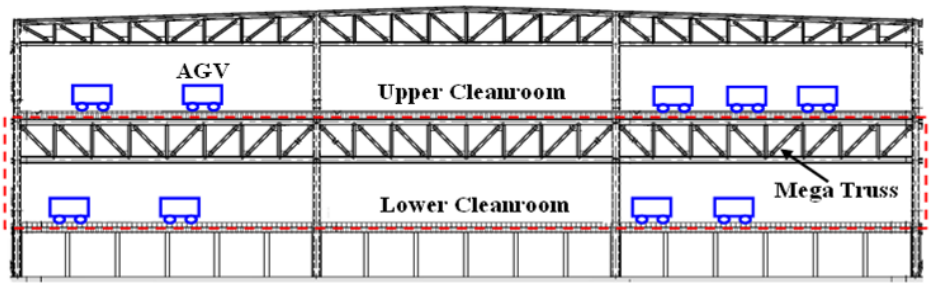

Fig. 3 Elevation view of typical double-cleanroom LCD building (Lee *et al*. 2012b)

Fig. 3 illustrates a typical double-fab LCD building with two clean rooms (Wang *et al*. 2003, Lee *et al*. 2012b), where a reinforced concrete (RC) waffle slab (Howard and Hansen 2003) supported by two-way grillage beams with a depth of 1.2 m, or a flat RC slab ("cheese" slab) with a thickness of 0.6 to 0.8 m supported by long-span steel mega trusses are often adopted in order to minimise the micro-vibration. The column span that supports the upper clean-room may vary from 19.2 m to more than 30 m, depending on the manufacturing generation of the mother glass size. The moving loads induced by AGVs that run in specific routes also apply directly to the long-span floors. The commercial finite element (FE) software such as ETABS (2002) or SAP2000 (2005) are often used to conduct the dynamic time history analysis of civil structures and facility buildings. Although the moving load analysis for bridges may be conducted by using the SAP2000, it may not be adequate for the analysis of the AGV-induced floor micro-vibration in LCD factories. The most popular types of floors built in LCD factories are the waffle slabs and cheese floors with the air ventilation holes. A large number of meshed floor elements is needed to construct the building models. In addition, high frequency vibration responses of up to 100 Hz are of interest as required by the tool manufacturers and users. Therefore, a significantly large number of vibration modes and an infinitesimal time interval are required to preserve the desired numerical stability and accuracy. Moreover, the moving pace of the AGVs in clean rooms is normally less than 2.0 m/s to prevent the glass panels from damage, implying the necessity to include a relatively long time duration in the analysis. These all together makes the analysis of the AGV-induced floor micro-vibration a time-consuming task. To simplify the task, Lee *et al*. (2012a, 2012b) proposed an equivalent simplified sub-structural multi-span continuous beam model to simulate the multi-span cheese floor of a single bay travelled by the AGV of a LCD factory without the need to construct a finite element model of the entire storey. The flexural rigidity was adjusted such that the fundamental frequency of the beam model is close to the in-situ measured first-mode floor vibration frequency. In these studies, the two-axle AGV was simulated as a pair of concentrated moving loads generated by a modified Kanai-Tajimi (MKT) power spectral density (PSD) function (Clough and Penzien, 1993, Yang and Agrawal 2000) considering various bandwidths. However, an identical AGV moving force PSD was used for different AGV moving speeds, which may not be a realistic assumption. Therefore, a more reasonable moving force pattern (intensity and bandwidth) corresponding to various vehicle weights and speeds should be developed for assessing the floor micro-vibration induced by AGVs moving with different conditions.

The moving force or contact force identification techniques that may be performed in time domain or frequency domain for vehicles moving on simply supported beams or multi-span

continuous bridges have been extensively studied and well developed over the last decade (Law *et al*. 1997, 1999, Chan *et al*. 1999, Chan *et al*. 2000, 2001a, b, Jiang *et al*. 2003, Yu and Chan 2003, 2007, Au *et al*. 2004, Chan *et al*. 2006, Deng and Cai 2010, 2011, Law and Zhu 2011). Among these studies, the unknown vehicle moving forces were normally identified through a beam element model (simulated as the lumped masses interconnected by massless beam elements), a continuous beam model (Euler's beam theory), or a finite element model, together with the simulated or experimental dynamic responses such as displacement, acceleration, bending moment, or strain time history data. The practical aspects in moving load identification such as measurement noise level, sampling frequency, number of vibration modes, number of measuring locations, road surface roughness and moving speed of vehicle were explored and discussed by Zhu and Law (2002). In addition to beam elements, the moving force identification was further extended for a simply supported orthotropic plate system by Law *et al*. (2007). Despite the fact that the moving force time histories could be identified by the proposed identification methods; however, the relationships between moving force spectra and both the vehicle weights and speeds were rarely further explored and constructed. If reasonable moving force spectra corresponding to various vehicle weights and speeds can be developed, the more reliable vehicle-induced responses of bridges or beams can be predicted. Therefore, this study intends to construct the relationships between moving force spectra and both the vehicle weights and moving speeds through a series of vehicle-induced vibration tests of a multi-span continuous steel beam model conducted in this study.

This study began with a series of vehicle-induced vibration tests of a small-scale three-span continuous steel beam model conducted in the laboratory to obtain a realistic moving load pattern (intensity and bandwidth) by using the experimental acceleration time history data. The best-fitting parameters that govern the MKT moving force PSDs under various vehicle static weights and moving speeds were then obtained through a regression analysis by using the experimentally identified moving force spectra. Finally, the floor micro-vibrations of a simplified sub-structural multi-span continuous beam model for a target LCD factory (Lee *et al*. 2012a, b) induced by AGV engine forces that were simulated by the proposed regressional MKT moving force PSDs for various AGV weights and moving speeds were assessed.

2. Theory of moving force identification

The equation of motion of a beam considering n vibration modes subjected to N concentrated moving loads can be represented as (Zheng *et al*. 1998, Lee *et al*. 2012a, 2012b)

$$\mathbf{M}\ddot{\mathbf{q}}(t) + \mathbf{C}\dot{\mathbf{q}}(t) + \mathbf{K}\mathbf{q}(t) = \mathbf{E}\mathbf{P}(t) \tag{1}$$

where $\mathbf{M} = [m_{ij}]$ is the $n \times n$ mass matrix, $\mathbf{C} = [c_{ij}]$ is the $n \times n$ damping matrix, $\mathbf{K} = [k_{ij}]$ is the $n \times n$ stiffness matrix, $\mathbf{q}(t) = \begin{bmatrix} q_1(t) \\ q_2(t) \\ \vdots \\ q_n(t) \end{bmatrix}$ is the $n \times 1$ modal displacement vector,

$$\mathbf{E}=\begin{bmatrix} X_1[x_{p1}(t)] & X_1[x_{p2}(t)] & \cdots & X_1[x_{pN}(t)] \\ X_2[x_{p1}(t)] & X_2[x_{p2}(t)] & \cdots & X_2[x_{pN}(t)] \\ \vdots & \vdots & \ddots & \vdots \\ X_n[x_{p1}(t)] & X_n[x_{p2}(t)] & \cdots & X_n[x_{pN}(t)] \end{bmatrix}$$ is the $n \times N$ location matrix of the moving loads on the beam, $\mathbf{P}(t)=\begin{bmatrix} P_1(t) \\ P_2(t) \\ \vdots \\ P_N(t) \end{bmatrix}$ is the $N \times 1$ moving load vector, and the mass and stiffness coefficients of the beam can be obtained as

$$m_{ij}=\int_0^L \rho A(x)X_i(x)X_j(x)dx \tag{2a}$$

$$k_{ij}=\int_0^L EI(x)X_i''(x)X_j''(x)dx \tag{2b}$$

where ρ is the density, E is the Young's modulus, $A(x)$ is the cross-sectional area, $I(x)$ is the moment of inertia of the cross-section, $X_i(x)$ is the ith vibration mode that satisfies the boundary conditions of the supports, and $X_i''(x)$ denotes the curvature of the ith vibration mode of the beam. It should be noted that the mode shapes of multi-span continuous beam adopted in this study are obtained by using the modified beam vibration functions (MBVF) as proposed by Zheng *et al*. (1998).

The vertical displacement of the beam, $w(x,t)$, can be represented as

$$w(x,t)=\sum_{i=1}^{n_s} q_{si}(t)X_i(x) \tag{3}$$

where n_s ($\leq n$) is the identified or available number of the vibration modes that are considered in calculating the dynamic responses, and $q_{si}(t)$ is the corresponding ith generalised coordinate. If the total number of accelerometers installed on a beam is η, then the acceleration response vector at sensor locations ($\overline{\mathrm{x}}=\begin{bmatrix} x_1 & x_2 & \cdots & x_\eta \end{bmatrix}^{\mathrm{T}}$) can be represented as

$$\begin{aligned} \ddot{\mathbf{w}}(\overline{\mathbf{x}},t)&=\begin{bmatrix} \ddot{w}(x_1,t) \\ \ddot{w}(x_2,t) \\ \vdots \\ \ddot{w}(x_\eta,t) \end{bmatrix}_{\eta\times 1} = \begin{bmatrix} X_1(x_1) & X_2(x_1) & \cdots & X_{n_s}(x_1) \\ X_1(x_2) & X_2(x_2) & \cdots & X_{n_s}(x_2) \\ \vdots & \vdots & \vdots & \vdots \\ X_1(x_\eta) & X_2(x_\eta) & \cdots & X_{n_s}(x_\eta) \end{bmatrix}_{\eta\times n_s} \begin{bmatrix} \ddot{q}_{s1}(t) \\ \ddot{q}_{s2}(t) \\ \vdots \\ \ddot{q}_{sn}(t) \end{bmatrix}_{n_s\times 1} \\ &=\overline{\mathbf{X}}\,\ddot{\mathbf{q}}_s(t) \end{aligned} \tag{4}$$

The modal acceleration vector can be obtained from the measured acceleration responses by using the pseudo-inverse (Borse 1997) as

$$\ddot{\mathbf{q}}_s(t) = \overline{\mathbf{X}}^{+}\ddot{\mathbf{w}}(\overline{\mathbf{x}},t) \tag{5a}$$

where $\overline{\mathbf{X}}^{+}$ is the pseudo-inverse of the mode shape matrix, $\overline{\mathbf{X}}$, at sensor locations. Similarly, the modal velocity and displacement vectors can be obtained, respectively, as:

$$\dot{\mathbf{q}}_s(t) = \overline{\mathbf{X}}^{+}\dot{\mathbf{w}}(\overline{\mathbf{x}},t) \tag{5b}$$

$$\mathbf{q}_s(t) = \overline{\mathbf{X}}^{+}\mathbf{w}(\overline{\mathbf{x}},t) \tag{5c}$$

Substituting Eqs. (5a), (5b) and (5c) into Eq. (1), the moving load vector can be identified as

$$\mathbf{P}(x = vt,t) = \mathbf{E}^{+}(\mathbf{M}\overline{\mathbf{X}}^{+}\ddot{\mathbf{w}}(\overline{\mathbf{x}},t) + \mathbf{C}\overline{\mathbf{X}}^{+}\dot{\mathbf{w}}(\overline{\mathbf{x}},t) + \mathbf{K}\overline{\mathbf{X}}^{+}\mathbf{w}(\overline{\mathbf{x}},t)) \tag{6}$$

in which $\mathbf{E}^{+}$ is the pseudo-inverse of the location matrix of the moving loads and it exists only when the number of vibration mode is smaller or equal to the number of sensors employed, $\mathbf{E}$, and v is the vehicle moving speed. It should be noted that the dimension of $\mathbf{E}$ in Eq. (6) would be $n_s \times N$.

The Eqs. (1) to (6) will be adopted later in Section 4.2 to identify the moving load time histories of a vehicle with two axles travelling on a three-span continuous steel beam model by using the experimental vibration response data obtained in the laboratory.

3. State-space procedure algorithm

The analytical solution to Eq. (1) of a beam system with zero initial conditions can be obtained by a recursive difference state-space equation as (Lopez-Almansa *et al*. 1988, Wang *et al*. 2001, Lee *et al*. 2012a, b)

$$\mathbf{z}[k+1] = \mathbf{A}\mathbf{z}[k] + \mathbf{E}_0\mathbf{P}[k] + \mathbf{E}_1\mathbf{P}[k+1] \tag{7}$$

In this equation, $\mathbf{z}[k+1] = \begin{bmatrix}\mathbf{q}[k+1]\\ \dot{\mathbf{q}}[k+1]\end{bmatrix}$ is the $2n \times 1$ state vector, $\mathbf{A} = e^{\mathbf{A}^*\Delta t}$ is the $2n \times 2n$ discrete-time system matrix, Δt is the sampling time, $\mathbf{A}^* = \begin{bmatrix}\mathbf{0} & \mathbf{I}\\ -\mathbf{M}^{-1}\mathbf{K} & -\mathbf{M}^{-1}\mathbf{C}\end{bmatrix}$ is the $2n \times 2n$ continuous-time system matrix, $\mathbf{E_0} = \left[(\mathbf{A}^*)^{-1}\mathbf{A} + \frac{1}{\Delta t}(\mathbf{A}^*)^{-2}(\mathbf{I}-\mathbf{A})\right]\mathbf{E}^*$ is the $2n \times N$ discrete-time moving load matrix of the previous time step, $\mathbf{E}_1 = \left[-(\mathbf{A}^*)^{-1} + \frac{1}{\Delta t}(\mathbf{A}^*)^{-2}(\mathbf{A}-\mathbf{I})\right]\mathbf{E}^*$ is the $2n \times N$ discrete-time moving load matrix of the current time step, and $\mathbf{E}^* = \begin{bmatrix}\mathbf{0}\\ -\mathbf{M}^{-1}\mathbf{E}\end{bmatrix}$ is the $2n \times N$ continuous-time moving load matrix.

Eq. (7) will be used to obtain the numerical vibration time histories of a three-span continuous

steel beam model subjected to the identified moving load time histories (Section 4.2), and those of a target TFT-LCD factory subjected to AGV moving loads simulated by the modified Kanai-Tajimi PSD function (Section 5.3).

4. Experimental setup and results

4.1 Experimental setup

In order to obtain the moving load pattern (intensity and bandwidth) induced by a vehicle with various weights and moving speeds, a series of dynamic tests for a small-scale three-span continuous steel beam model with a width of 0.15m and a total length of 3m (Fig. 4) were conducted in the laboratory. The accelerometers (Model: 352C68, frequency range: 0.5 to 10000 Hz, PCB PIEZOTRONICS) were installed at the central and one-quarter locations of each span of the beam to monitor the vertical acceleration time histories induced by a two-axle vehicle. As a result, acceleration time histories at six sensor locations were obtained synchronously in this study. The moving speed of the two-axle vehicle was controlled by using motors with different revolutions per minute (RPM) of 60, 150, 200, and 400, and the vehicle weight was simulated by using mass blocks with W = 13.00 N, 19.98 N, 24.97 N, 33.71 N, and 40.45 N in the experiment.

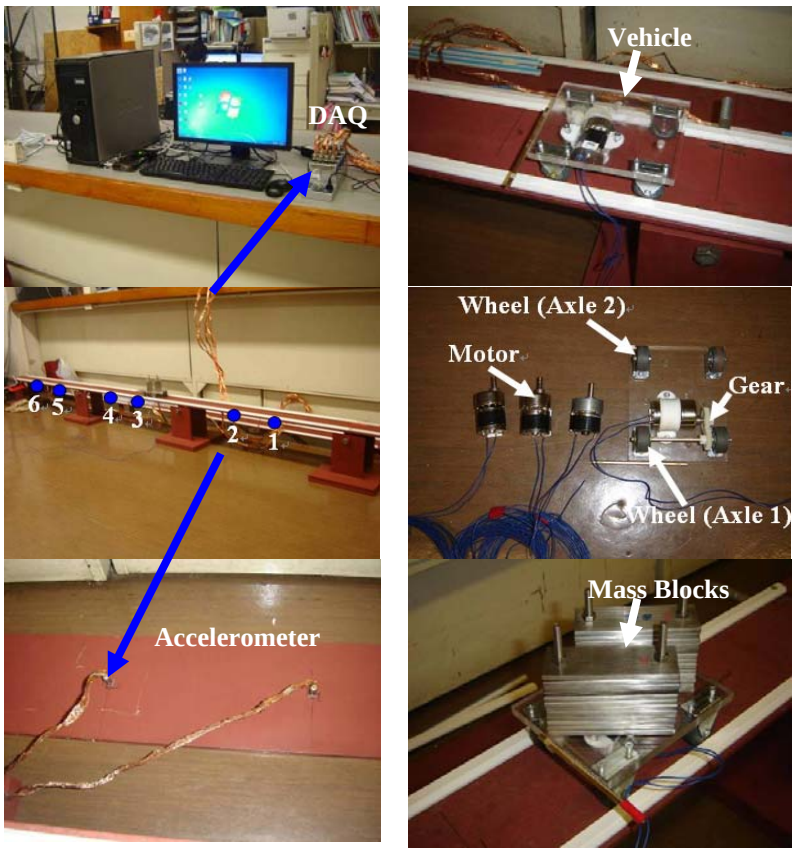

Fig. 4 Experimental setup of vehicle-induced floor vibration tests

4.2 Experimental results

As shown in Eq. (6), the dynamic moving forces of a vehicle can be obtained by using the acceleration, velocity and displacement responses of a beam. In this study, the vertical acceleration response ($\ddot{\mathbf{w}}(\bar{\mathbf{x}},t)$) of the three-span continuous steel beam was obtained directly from the experimental tests, while the velocity ($\dot{\mathbf{w}}(\bar{\mathbf{x}},t)$) and displacement ($\mathbf{w}(\bar{\mathbf{x}},t)$) responses were numerically computed by integrating the acceleration response with respect to time, once and twice, respectively. It should be noted that the frequency contents of the experimental acceleration response below the frequency of 3.0 Hz were filtered out before performing the integration. The frequency of 3.0 Hz is far from the first natural (predominated) frequency (14.063 Hz) of the three-span continuous steel beam model; therefore, less predominated acceleration response would be filtered out, whereas the numerical stable and accurate integrated velocity and displacement time histories can be achieved. Moreover, n_s = 4 (modes) was used when performing the moving force identification and the dynamic analysis of the three-span continuous steel beam model. It should be noted that a mass per unit length of ρA = 7.0740 kg/m and a flexural rigidity of EI = 567 N-m^2 of the continuous beam model were determined based on a cross-sectional dimension of 0.15m × 0.006m, so that the four natural vibration frequencies were found to be 14.063 Hz, 18.021 Hz, 26.725 Hz, and 81.631 Hz from eigen-analysis of the mass and stiffness matrices (Eqs. (2a) and 2(b)). Moreover, a 3% damping ratio is assumed for each vibration mode.

Fig. 5 shows the experimental vertical acceleration time histories monitored at six locations of the three-span continuous steel beam model, in which the sampling period is 6.05×10^{-4} s, and the average moving speed of the vehicle with W = 40.45 N driven by a 400-RPM motor, is 0.55m/s. Due to the paper length limitation, only partial experimental results are presented in this paper.

Fig. 6(a) presents the comparisons of beam vibration spectra induced by the vehicle with W = 40.45 N moving at various speeds, in which the vibration tends to increase with the vehicle speed in the higher frequency range regardless of the measurement locations. The comparisons of vibration spectra induced by the vehicle with various weights driven by a 400-RPM motor are shown in Fig. 6(b), in which the vibration tends to slightly increase with the vehicle weight in the lower frequency range regardless of the measurement locations. The results demonstrate that the vehicle weight and moving speed may have significant effects on beam vibrations due to different frequency contents of vehicle moving loads. It should be noted that in order to obtain the clearer vibration spectral trend of the relatively stiffer continuous steel beam model under various vehicle weights and speeds, the larger vehicle weights within the range of 6% to 19% of the total beam weight were used in this study.

Fig. 7 shows the identified dynamic moving force time histories of axle 1 obtained by using Eq. (6) for a vehicle with various weights driven by a 400-RPM motor. The moving forces are found to be more significant as vehicle moves toward the intermediate supports of the three-span continuous steel beam near which the mode shape values are close to zero. As a result, the numerical singularity problem may occur due to the use of the pseudo-inverse of the location matrix of the moving loads, $\mathbf{E}^+$, which was computed based on the singular value decomposition (SVD) method (Borse 1997). In order to obtain numerically stable results, a tolerance value of 0.28 was used in this study such that any singular values less than the tolerance value were treated as zero. It should be noted that any value between 0.10 and 0.28 could be selected as the tolerance value to obtain the stable numerical results in this case. If the identified dynamic moving forces of the two axles (N = 2) are substituted into Eq. (7), the numerical acceleration response at the central

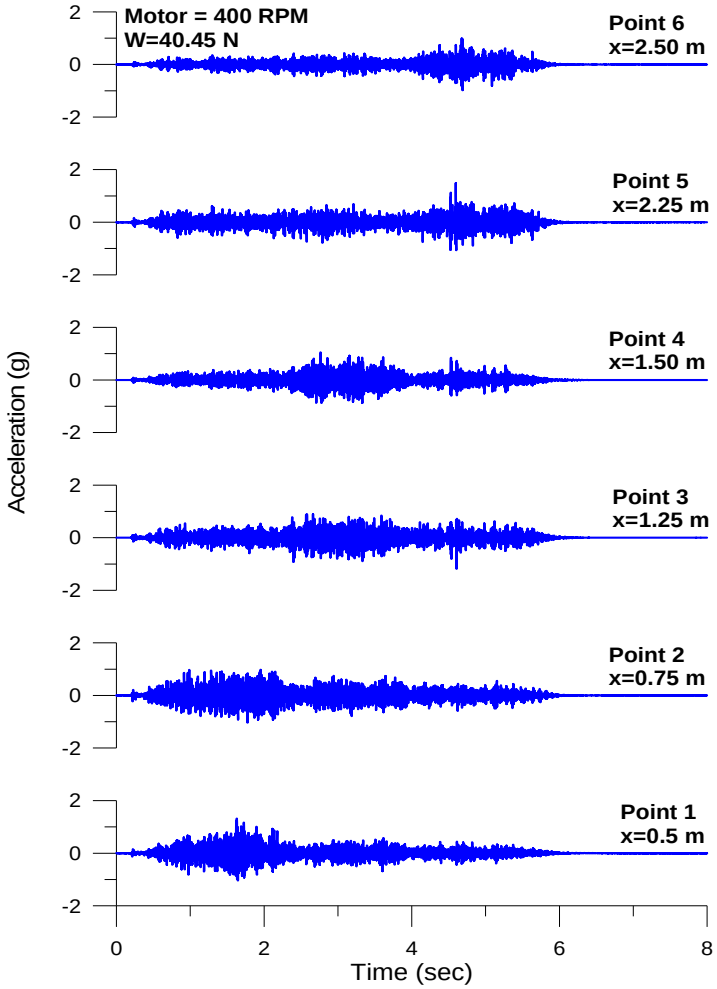

Fig. 5 Experimental acceleration time histories monitored at six locations (RPM = 400 and W = 40.45 N)

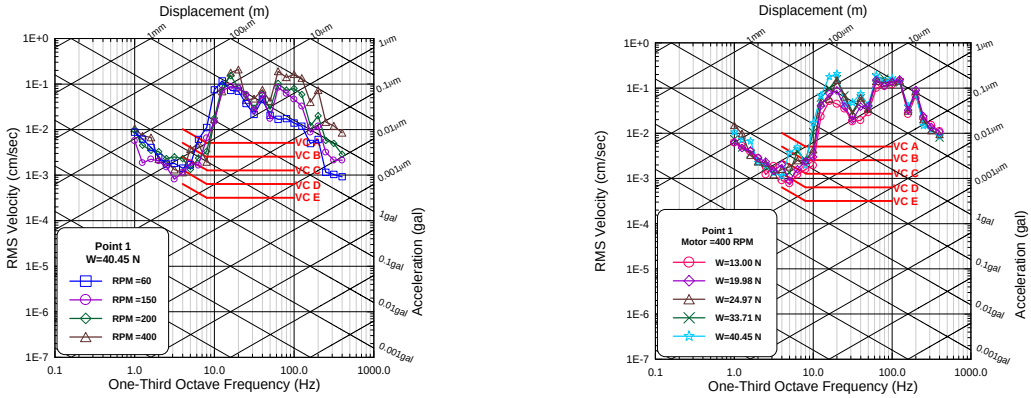

Fig. 6 Comparisons of vibration spectra: (a) various moving speeds (W = 40.45 N); (b) various vehicle weights (RPM = 400)

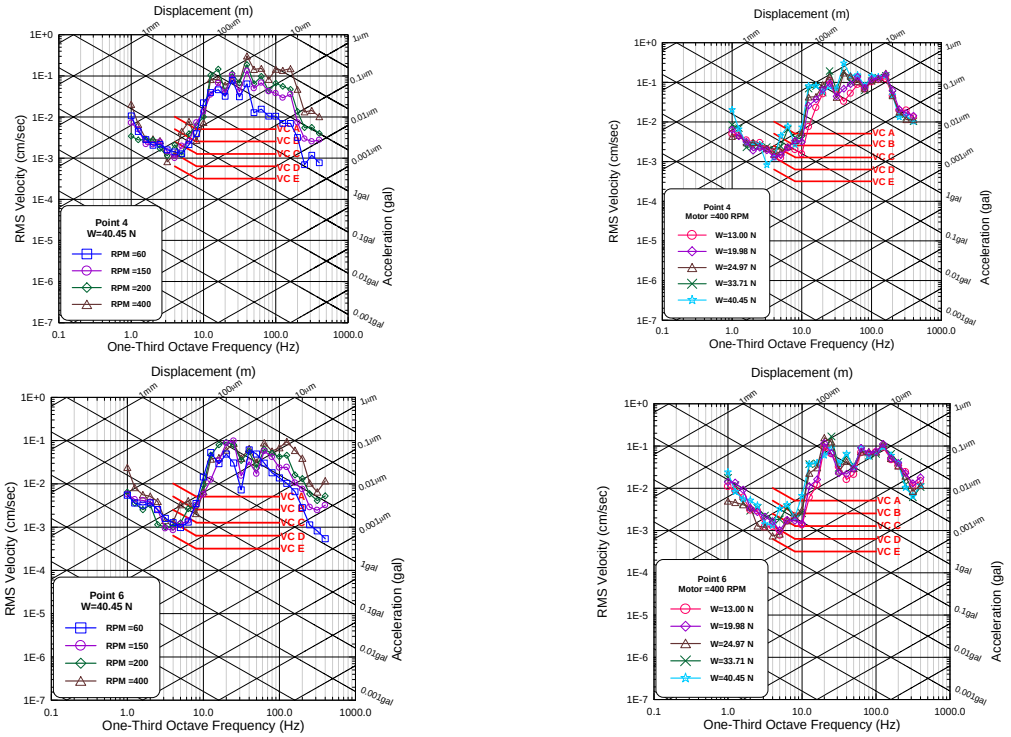

Fig. 6 Continued

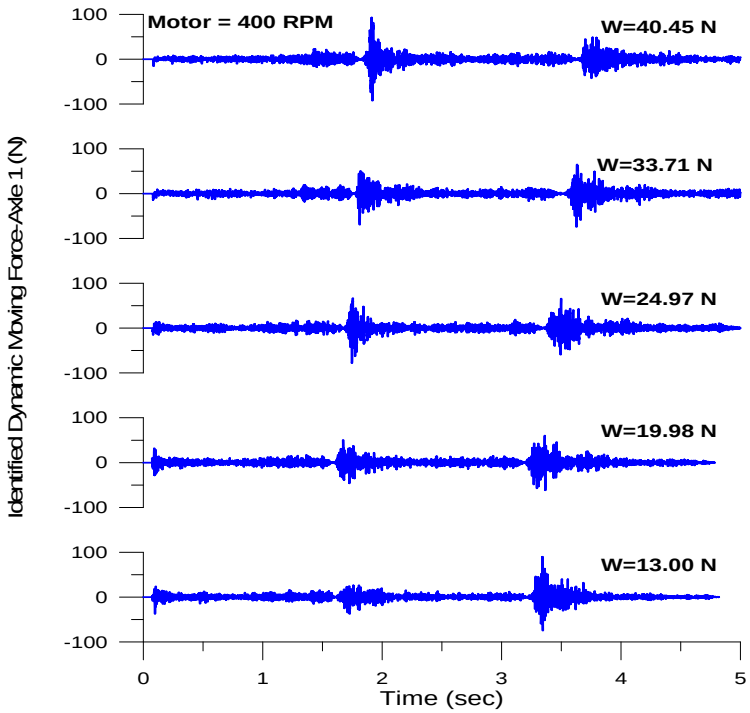

Fig. 7 Identified dynamic moving force time histories of axle 1 (RPM = 400)

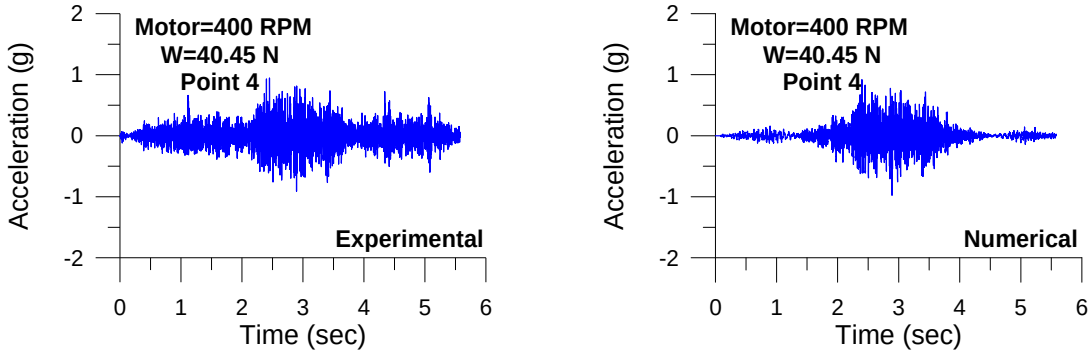

(a)

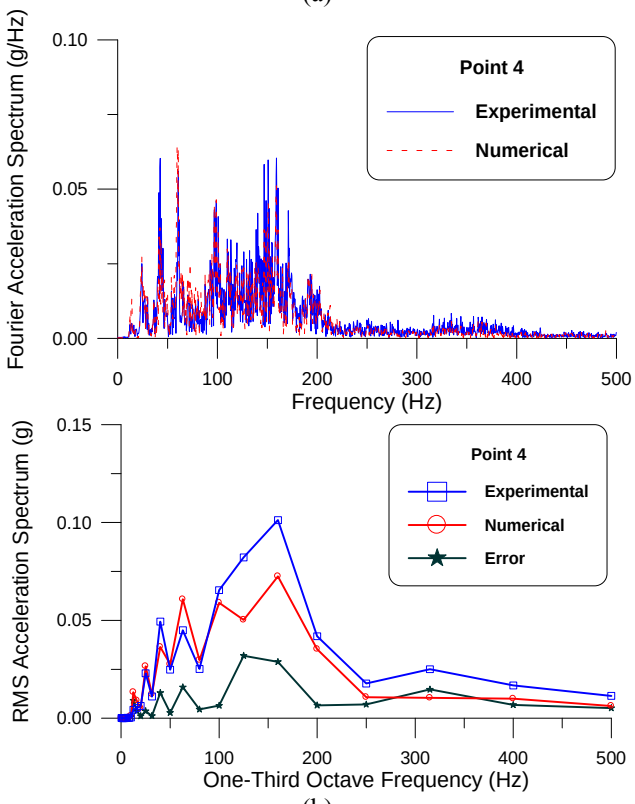

(b)

Fig. 8 Comparisons of experimental and numerical acceleration response at point 4 (RPM=400 and W = 40.45 N): (a) time histories; (b) spectra

location of the middle span (point 4) of the three-span continuous steel beam model can be obtained by the SSP algorithm and shown in Fig. 8(a). In order to investigate the accuracy of the numerical random vibration response, the Fourier acceleration spectra were further transformed to the RMS acceleration spectra in one-third octave frequency band (Fig. 8(b)), which is a more concise spectrum format in the engineering application as compared to the Fourier spectrum. Moreover, a global error index (GEI) is defined herein as the ratio of the sum of the squares of the RMS acceleration error to the sum of the squares of the experimental RMS acceleration as

$$\mathrm{GEI} = \frac{\sum_{i=1}^{n_f} [RMS_e(f_{ci}) - RMS_n(f_{ci})]^2}{\sum_{i=1}^{n_f} RMS_e(f_{ci})^2} 100\% \tag{8}$$

in which f_{ci} is the ith centre frequency (Gordon 1991) defined in the one-third octave frequency band, RMS_e is the experimental RMS acceleration, RMS_n is the numerical RMS acceleration obtained using the identified moving force, and n_f is the maximum number of the centre frequency considered. The GEI at point 4 of the case of RPM = 400 and W = 40.45 N as shown in Fig. 8(b) is 9.12%, in which we can find that the major difference between the experimental and numerical RMS acceleration spectra is from the frequency contents above 100 Hz. This result is reasonable because only the first four vibration modes (n_s = 4) with the highest frequency of 81.631 Hz was used in the numerical simulation. In the series of vehicle-induced beam vibration tests conducted in this study, the maximum GEI of 13.07%, the minimum GEI of 7.48% and the average GEI of 10.96% at point 4 were obtained from the error surface as shown in Fig. 12(a). This indicates that the dynamic moving force (or engine force) time histories can be identified by using the experimental acceleration time histories data with satisfactory accuracy.

4.3 Regression analysis of the modified Kanai-Tajimi model

A modified Kanai-Tajimi (MKT) power spectral density (PSD) function (Clough and Penzien 1993, Yang and Agrawal 2000) is adopted in this study to simulate the vehicle moving forces (or engine forces) in a frequency-domain format as

$$F(f) = \frac{[1 + 4\xi_1^2 (f/f_1)^2](f/f_2)^2 S_0^2}{\{[1-(f/f_1)^2]^2 + 4\xi_1^2 (f/f_1)^2\}\{[1-(f/f_2)^2]^2 + 4\xi_2^2 (f/f_2)^2\}} \tag{9}$$

where f_1, ξ_1, f_2 and ξ_2 are the constant parameters (where f_1 and f_2 control the upper bound and lower bound of the predominant bandwidth of the moving force, respectively), and S_0 is the force intensity. The best-fitting parameters of the MKT model such as the lower-bounded frequency f_2 and the moving force intensity S_0, can be obtained by using the identified moving force spectra and a given upper-bounded frequency f_1. It should be noted that S_0^2 used in this study is a constant PSD function, which represents white noise. Therefore, the moving force PSD with a desired bandwidth and intensity can be obtained by modulating a white noise signal through the MKT filtering functions in terms of f_1, ξ_1, f_2, ξ_2 and S_0.

The identified one-sided dynamic moving force PSD can be obtained as

$$P_{ss}(f) = \frac{2\,|P_s(f)|^2}{T} \tag{10}$$

in which $P_s(f)$ is the Fourier transform of the identified dynamic moving force time history $P(t)$, and T is the total duration of the history data.

This study further computes the one-third octave band RMS moving force spectra as (Amick and Bui 1991, Yang and Agrawal 2000)

$$P_{1/3}(f_{ci}) = \sqrt{\sum_{0.89 f_{ci}}^{1.12 f_{ci}} P_{ss}(f)\Delta f} \tag{11}$$

in which $0.89f_{ci}$ and $1.12f_{ci}$ are, respectively, the lower-bounded and upper-bounded frequencies of the bandwidth ($0.23f_{ci}$) for the ith centre frequency, and Δf is the resolution (or frequency interval) of the Fourier spectrum $P_s(f)$. The relationship between the i+1th and ith centre frequencies can be represented as $f_{ci+1} = 2^{1/3} f_{ci}$. For instance, if the first centre frequency is f_{c1} = 1 Hz, the corresponding lower-bounded and upper-bounded frequencies are 0.89 Hz and 1.12 Hz, respectively; the second centre frequency can be obtained as $f_{c2} = 2^{1/3} \times 1 = 1.25$ Hz, and the corresponding lower-bounded and upper-bounded frequencies are 1.12 Hz and 1.41 Hz, respectively.

Fig. 9(a) shows the identified one-third octave band RMS moving force spectra of the two -axle vehicle with RPM = 400 and W = 40.45 N, in which the upper-bounded frequency of the predominate bandwidth is found to be around 160 Hz. Therefore, the parameter f_1 of the MKT model is fixed to be 160 Hz. In order to obtain an optimal lower-bounded frequency f_2 of the MKT moving force PSD, the sum of the squares of the error between the experimental and MKT-simulated RMS moving force spectra for each centre frequency within 160 Hz is computed by varying f_2. The value f_2 that minimises the sum of the squares of the error is the optimal lower-bounded frequency. It should be noted that the parameters, ξ_1, ξ_2, and S_0 are manually adjusted when obtaining the sum of the squares of the error with the varying parameter f_2.

The optimal lower-bounded frequencies of the MKT model for the axle 1 and axle 2 are f_2 = 72 Hz (with ξ_1 = 0.20, ξ_2 = 0.15, and S_0 = 0.10) and f_2 = 77 Hz (with ξ_1 = 0.15, ξ_2 = 0.17, and S_0 = 0.10), respectively, at which the sums of the squares of the error are minima, as shown in Fig. 9(b). Moreover, the experimental and MKT-PSD-simulated one-third octave band RMS moving force spectra have shown to be consistent as illustrated in Fig. 9(a). The MKT moving force PSDs simulated by the aforementioned parameters for the two-axle vehicle with RPM = 400 and W = 40.45 N are presented in Fig. 9(c).

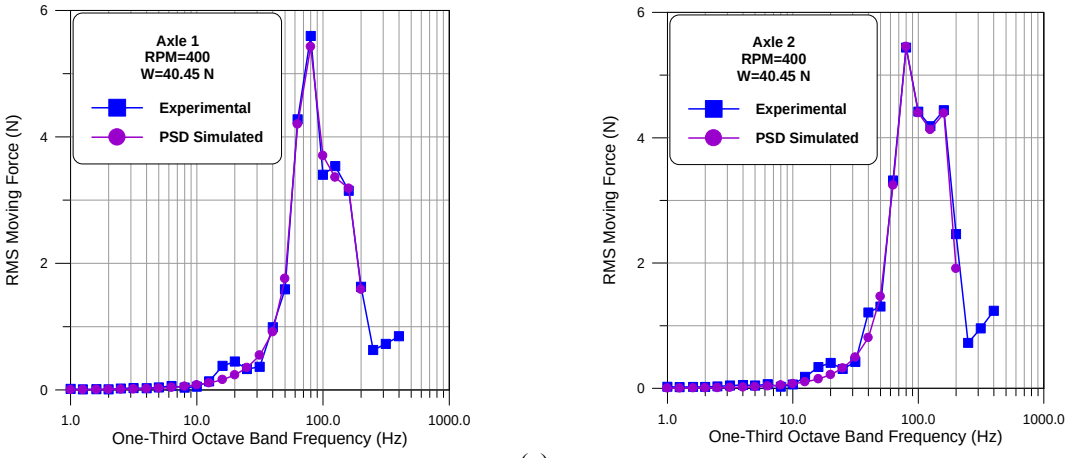

(a)

Fig. 9 MKT model: (a) RMS moving force spectra; (b) sum of the squares of the error with f_2; (c) best-fitting PSDs

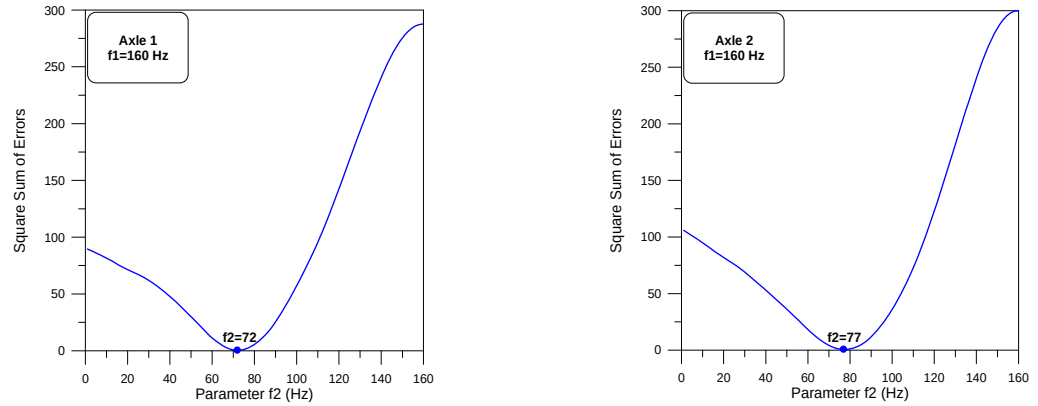

(b)

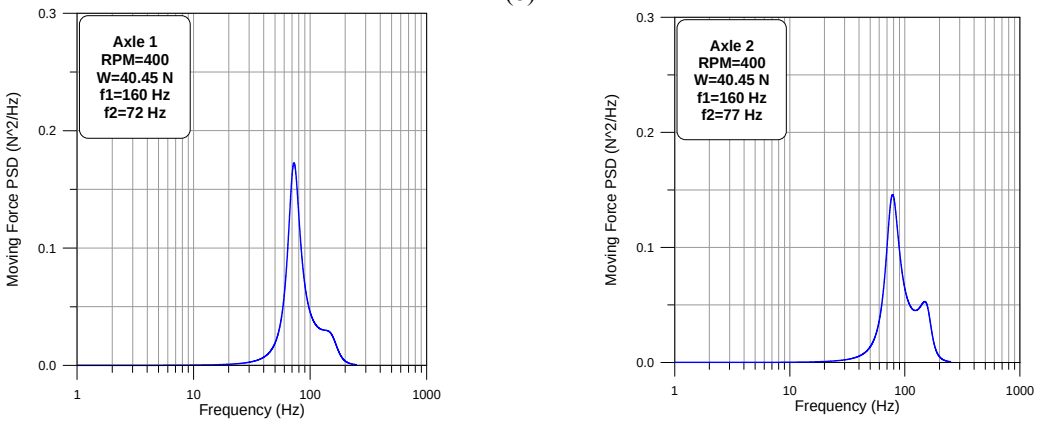

(c)

Fig. 9 Continued

If all the parameters of the MKT model corresponding to various vehicle weights and speeds are obtained, a regressional MKT model can be further constructed. From the experimental tests conducted in this study, we obtained a maximum upper-bounded frequency f_1 of 160 Hz, a maximum vehicle weight $W_{\max}$ of 40.45 N, a maximum vehicle speed $v_{\max}$ of 0.63 m/s (for the case with W = 19.98 N and RPM = 400), and a maximum moving force intensity $S_{0\max}$ of 0.10. Moreover, by introducing the dimensionless parameters such as the normalised lower-bounded frequency defined as $\bar{f}_2 = f_2/f_1$, the normalised intensity as $\bar{S}_0 = S_0/S_{0\max}$, the normalised weight as $\overline{W} = W/W_{\max}$, and the normalised speed as $\bar{v} = v/v_{\max}$, the identified $\bar{f}_2$ and $\bar{S}_0$ with $\overline{W}$ and $\bar{v}$ for the axle 1 of the vehicle are shown in Fig. 10(a) and Fig. 11(a), respectively. The best-fitting equations associated with the identified dimensionless parameters of the MKT model can be obtained by performing a regression analysis and summarised as

$$\bar{f}_2 = 0.3471 - 0.3342\overline{W} + 0.7260\bar{v} + 0.1774\overline{W}^2 - 0.3988\bar{v}^2 - 0.1040\overline{W}\bar{v} \text{ (Axle 1)} \quad (12a)$$

$$\bar{f}_2 = 0.4428 - 0.3485\overline{W} + 0.2977\bar{v} + 0.1628\overline{W}^2 - 0.1728\bar{v}^2 + 0.0811\overline{W}\bar{v} \text{ (Axle 2)} \quad (12b)$$

$$\overline{S}_0 = -0.1133 + 0.4327\overline{W} + 0.5277\overline{v} - 0.4068\overline{W}^2 - 0.0585\overline{v}^2 + 0.6940\overline{W}\overline{v} \text{ (Axle 1)} \quad (13a)$$

$$\overline{S}_0 = -0.1315 + 0.4066\overline{W} + 0.6507\overline{v} - 0.3513\overline{W}^2 - 0.0584\overline{v}^2 + 0.5850\overline{W}\overline{v} \text{ (Axle 2)} \quad (13b)$$

The regressional $\bar{f}_2$ and $\overline{S}_0$ with $\overline{W}$ and $\overline{v}$ for the axle 1 of the vehicle are shown in Fig. 10(b) and Fig. 11(b), respectively. From the regressional Eqs. (12) and (13), the normalised lower-bounded frequency $\bar{f}_2$ and the normalised intensity $\overline{S}_0$ of the MKT moving force model for specific weight and speed of a vehicle can be determined.

Fig. 12(a) illustrates the error (GEI as defined in Eq. (8)) surface at point 4 for the case with the excitation as the identified moving force, from which the maximum GEI of 13.07%, the minimum GEI of 7.48% and the average GEI of 10.96% are obtained. Similarly, the error surface at point 4 for the case with the excitation as the MKT-simulated moving force is illustrated in Fig. 12(b), in which the maximum, the minimum and the average GEIs are 19.43%, 7.08 and 12.03%, respectively. The maximum error between the results shown in Figs. 12(a) and 12(b) is 9.35%, which indicates that the moving force patterns for various vehicle weights and speeds in this experimental study can be numerically simulated by the MKT model with satisfactory accuracy if the proper parameters, such as $\bar{f}_2$ and $\overline{S}_0$, determined from the proposed regressioanl Eqs. (12) and (13), together with $\xi_1 = 0.10$ and $\xi_2 = 0.30$ are used. This study will adopt the similar moving load pattern as the proposed regressional MKT model to simulate the AGV engine forces when conducting the dynamic analysis of AGV-induced floor micro-vibrations in LCD factory as will be explored later.

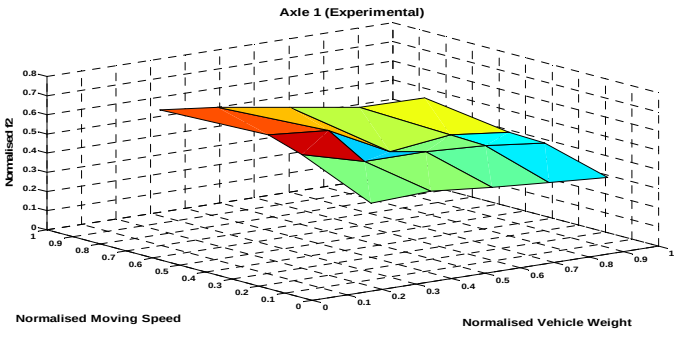

(a)

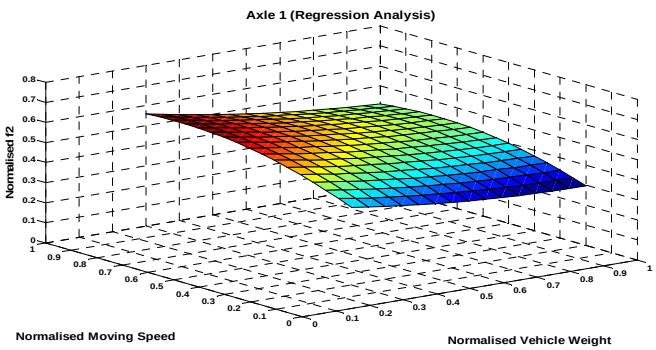

(b)

Fig. 10 The normalised lower-bounded frequency $\bar{f}_2$ of the MKT model (Axle 1): (a) experimental; (b) regression analysis

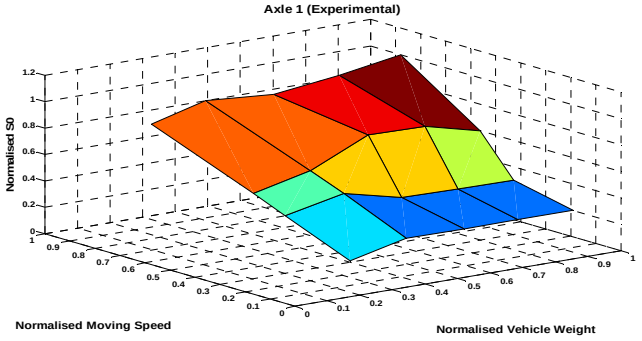

(a)

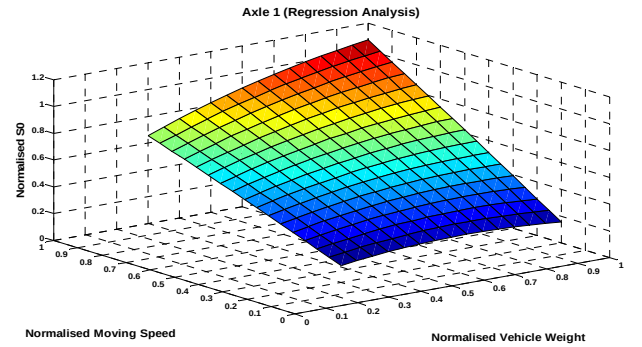

(b)

Fig. 11 The normalised intensity $\overline{S}_0$ of the MKT model (Axle 1): (a) experimental; (b) regression analysis

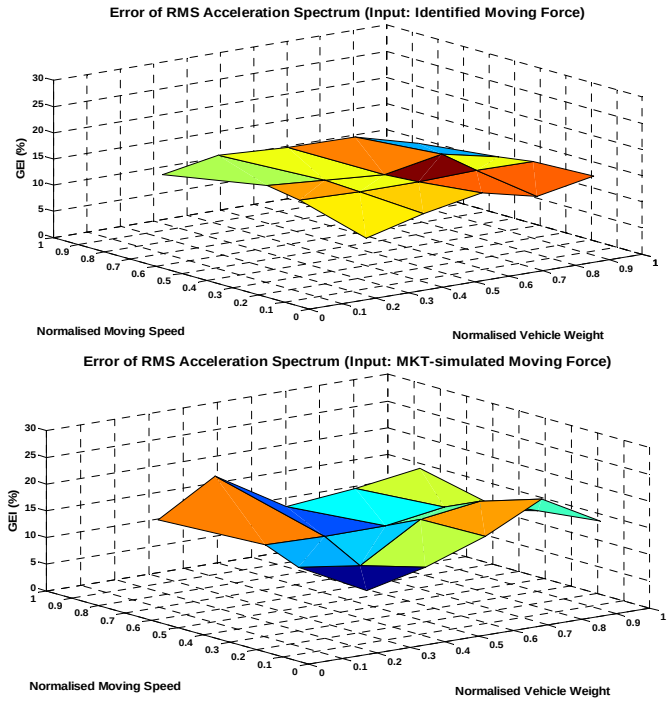

Fig. 12 The GEI of RMS acceleration spectra at point 4: (a) input: identified moving force; (b) input: MKT-simulated moving force

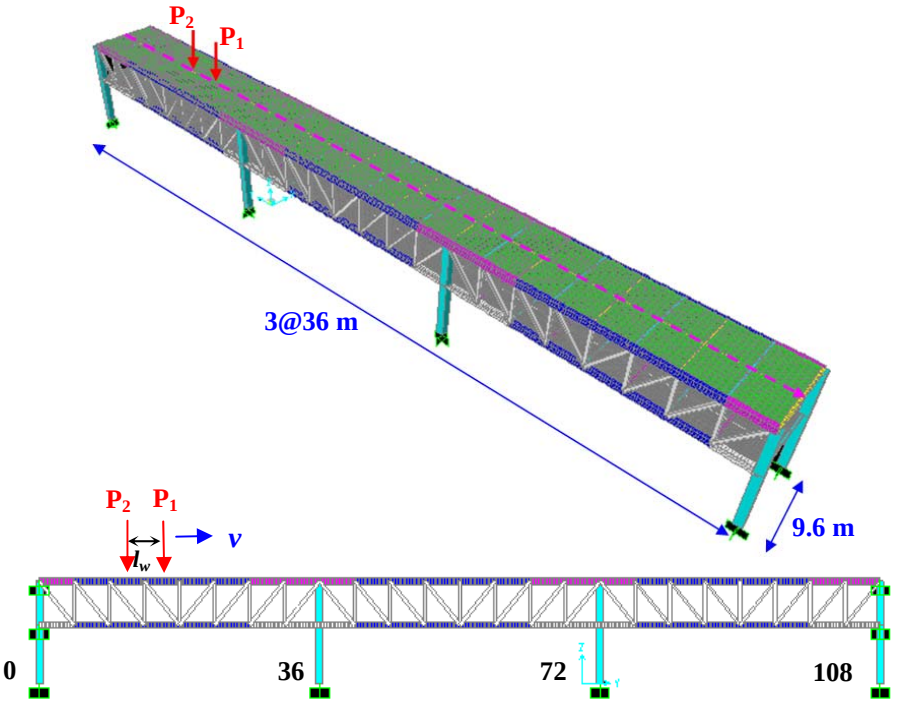

Fig. 13 Illustration of AGV moving loads on an equivalent three-span beam model

5. Assessment of AGV-induced floor micro-vibration

5.1 The target LCD factory

The LCD facility building illustrated in Fig. 3 is considered in the study. Since the vertical floor vibration is in essence a localised behaviour of the structure, and the vibration is most pronounced along the AGV moving bay, a simplified sub-structural three-span continuous beam model subjected to moving loads (Fig. 13) is considered to be adequate (Lee *et al*. 2012a, b) and adopted in this study. The mega truss spans 36 m equally in each bay with a width of 9.6 m. It supports a RC cheese slab with a thickness of 0.55 m, giving a mass per unit length of $\rho A = 9.1505 \times 10^3$ kg/m and an equivalent flexural rigidity of $EI = 2.3097 \times 10^{11}$ N-m^2 (Lee *et al*. 2012a), so that the first five natural frequencies of the equivalent three-span continuous beam determined from eigen-analysis of the mass and stiffness matrices are 6.089 Hz, 7.804 Hz, 11.395 Hz, 24.357 Hz, and 27.759 Hz. Moreover, a 5% damping ratio is assumed for each vibration mode.

5.2 Simulation of AGV engine forces

In order to assess AGV-induced long-span floor micro-vibrations under various AGV weights and moving speeds in the target LCD factory, this study takes into account the total static weight of the AGV with $W = 21582$ N (mass = 2200 kg), 17265.6 N (mass = 1760 kg), 12949.2 N (mass = 1320 kg), 8632.8 N (mass = 880 kg), and 4316.4 N (mass = 440 kg), and the moving speed of the AGV with $v = 2.0$ m/s, 1.5 m/s, 1.0 m/s, and 0.5 m/s when performing the dynamic analysis.

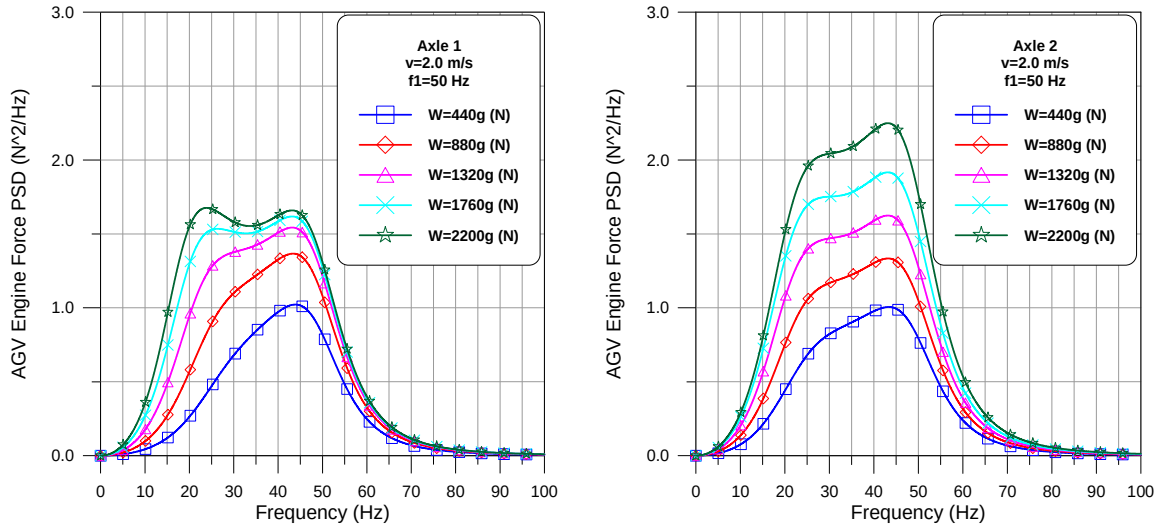

Fig. 14 Simulated AGV Engine force PSDs for various AGV weights (v = 2.0 m/s)

Moreover, the upper-bounded frequency of the AGV engine force frequency contents is conservatively considered as f_1 = 50 Hz. From the abovementioned parameters, we obtain the normalised AGV weights as $\overline{W}$ =1.0, 0.8, 0.6, 0.4, and 0.2, and the normalised AGV speeds as $\bar{v}$ =1.0, 0.75, 0.5, and 0.25. Substituting $\overline{W}$ and $\bar{v}$ into Eqs. (12) and (13), the normalised lower-bounded frequencies and the normalised intensities of the MKT engine force PSDs can be obtained. Taking $\bar{v}$ = 1.0 as an example, the normalised lower-bounded frequencies of the axle 1 for $\overline{W}$ = 1.0, 0.8, 0.6, 0.4, and 0.2 are determined from Eq. 12(a) as $\bar{f}_2$ = 0.4135 (f_2 = 50 × 0.4135 = 20.68 Hz), 0.4373 (f_2 = 21.87 Hz), 0.4752 (f_2 = 23.76 Hz), 0.5274 (f_2 = 26.37 Hz), and 0.5938 (f_2 = 29.69 Hz), respectively. Therefore, the MKT engine force PSDs for AGVs with various weights and v = 2.0 m/s can be obtained from Eq. (9) and illustrated in Fig. 14, in which S_0 = 1.0, ξ_1 = 0.23 and ξ_2 = 0.51 are used. It is seen that both the moving force intensity and bandwidth vary and increase with the AGV weight and moving speed, which is believed to be a reasonable model in simulating moving force spectra. With these PSD functions, the corresponding time histories can be generated as (Shinozuka 1971)

$$F(t) = \sqrt{2}\sum_{i=1}^{N_f}\sqrt{F(f_i)\Delta f}\,\cos(2\pi f_i t + \phi_i) \tag{14}$$

in which N_f is the number of frequency interval, $F(f_i)$ is the modified Kanai-Tajimi PSD value (Eq. 9) at ith discretised frequency $f_i = i\Delta f$, and ϕ_i is the random phase angle with a uniform distribution between 0 and 2π.

Fig. 15 shows the AGV engine force time histories for various AGV weights under v. 2.0 m/s as simulated by using Eq. (14). It should be noted that the AGV engine force time histories were obtained by using the regressional MKT PSDs of the axle 2 (Fig. 14) and the maximum engine force was scaled to be around 2943 N (equivalent to mass=300 kg) for this type of AGV (Lee *et al.* 2012b).

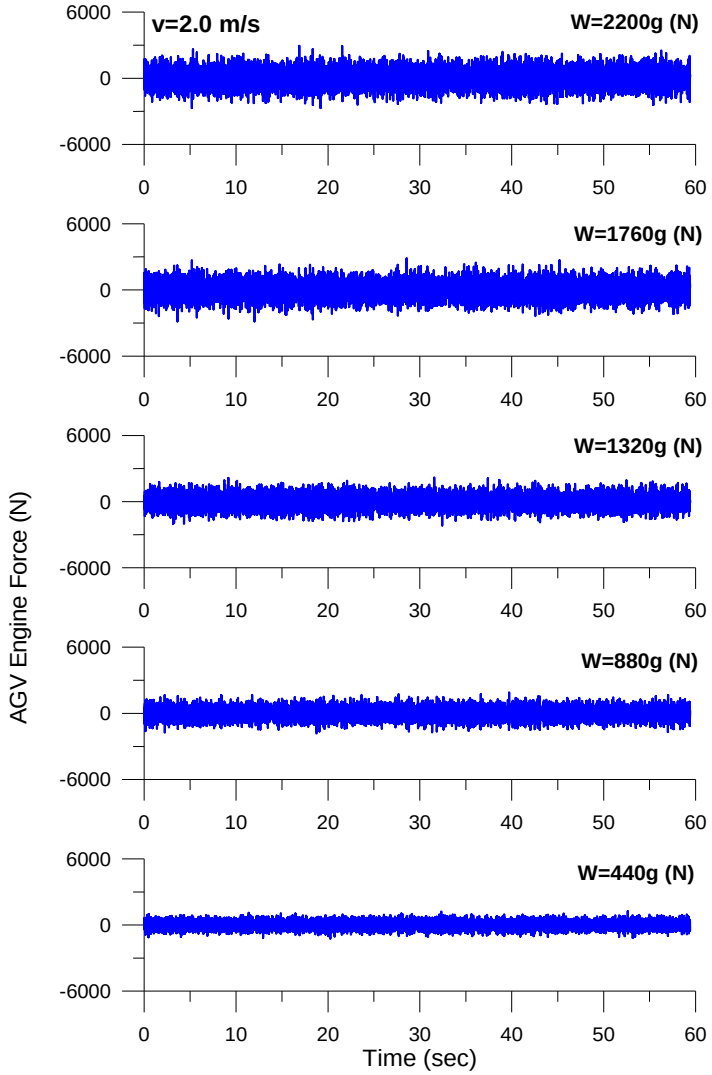

Fig. 15 Simulated AGV engine force time histories for various AGV weights (v = 2.0 m/s)

5.3 Assessment of AGV-induced floor vibration levels

In this study, the micro-vibrations induced by a single AGV with various weights and moving speeds on the sub-structural three-span continuous beam model is assessed by the SSP algorithm considering n = 12 modes. The AGV is simulated as a pair of concentrated moving loads of $P_1(t) = P_2(t) = W/2 + F(t)/2$ separated at an axle distance of l_w = 1.2 m. The simulated engine force time histories $F(t)$ of AGVs with various weights moving at v. 2.0 m/s as shown in Fig. 15 (with a time interval of 0.001 s) are used in this study. Moreover, for simplicity, the AGV engine force time histories of the two axles are assumed to be identical.

Fig. 16 demonstrates the simulated central floor micro-vibration spectra of the middle span (x = 54 m) under various moving speeds of an AGV with W = 21582 N. It is seen that the floor micro-

vibration increases with AGV moving speed, and the maximum micro-vibration level falls within the VC-D and VC-C levels when AGV moves at a lower speed of 0.5 m/s, while they may reach the VC-B level when AGV moves at a higher speed of 1.5 m/s. In addition to the central location of the middle span, the floor micro-vibrations along the part of floor travelled by the AGV are further explored. Fig. 17 shows the maximum vertical floor velocity ratios (VRs) at various locations (6 m uniformly-spaced, except at the supports) of the three-span continuous beam subjected to AGV moving loads. It is noted that the maximum VR is defined as the ratio of overall maximum AGV-induced one-third octave band RMS velocity to the VC-E level of 3.175×10^{-4} cm/s. Generally speaking, the floor micro-vibrations increase with the AGV weight and moving speed. The micro-vibrations may fall within the VC-D and VC-C levels when the AGV with $W \geq$ 8633 N moves at a lower speed of 0.5 m/s, while they may exceed the VC-C level as required for the installation of most stringent vibration-sensitive tools when the AGV with $W \geq 8633$ N moves at a speed of 1.0 m/s. As AGV moves at a speed higher than 2.0 m/s, the micro-vibrations may exceed the VC-B level, except for the case of AGV with $W \leq 4136$ N. The simulated vertical micro-vibration levels of the long-span floor system in the target LCD factory are comparable to the maximum micro-vibration levels of typical LCD factories (larger than the VC-B level or even exceeding the VC-A level as shown in Fig. 2) induced by AGVs moving normally at a speed between 1.0 m/s and 2.0 m/s. Hence, the dynamic algorithm that integrates the sub-structural multi-span continuous beam model and the proposed regressional MKT AGV moving force (engine force) model taking various AGV static weights and moving speeds into account, are considered adequate and reliable in assessing the AGV-induced floor micro-vibration levels in LCD factories.

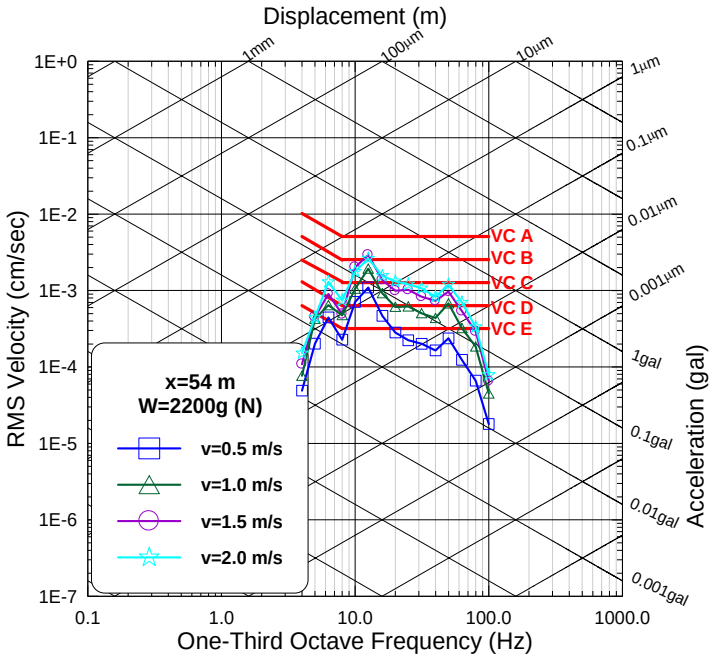

Fig. 16 AGV-induced floor micro-vibration spectra at central location of middle span under various AGV speeds (W = 21582 N, x = 54 m)

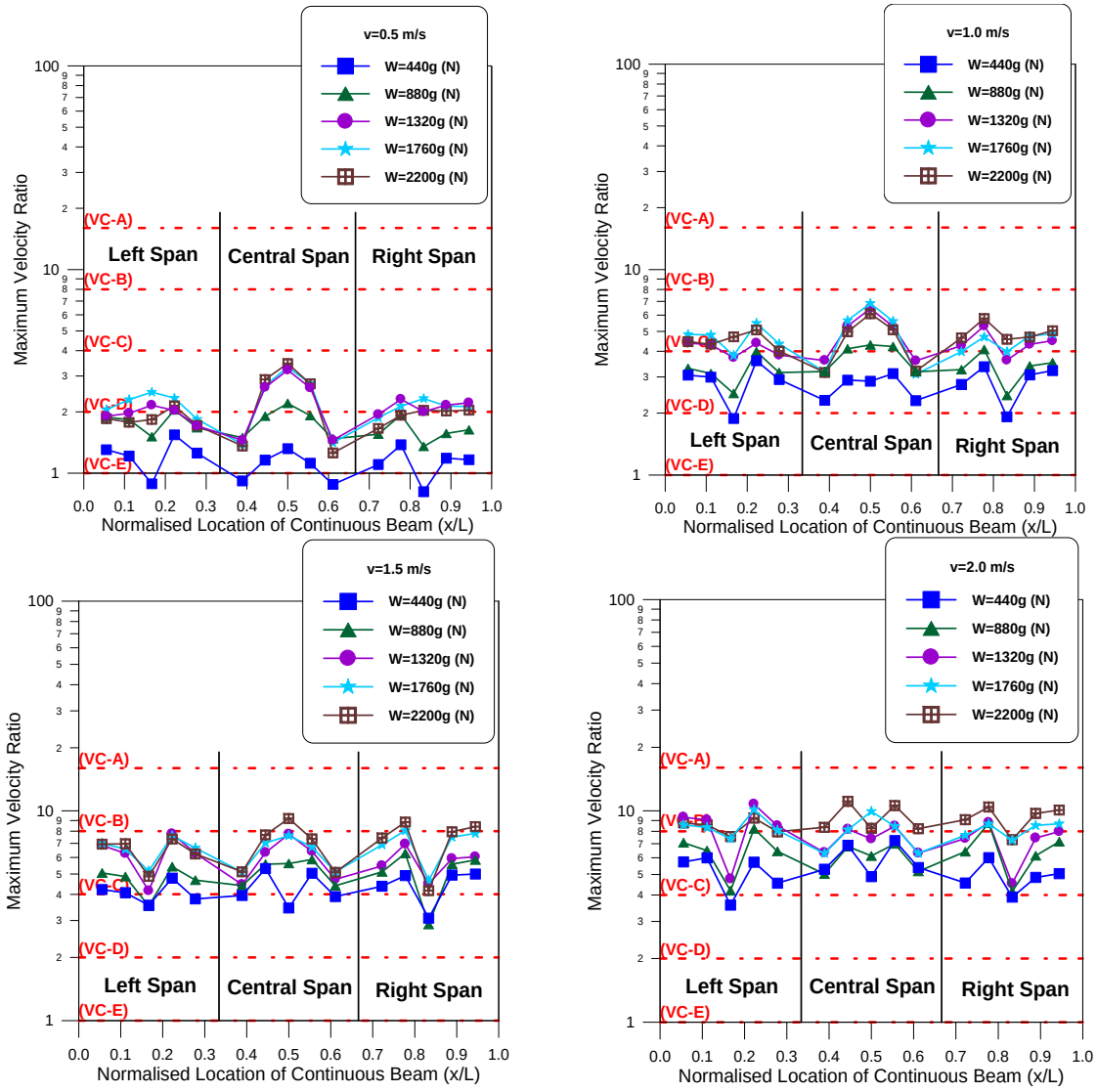

Fig. 17 Maximum velocity ratios at various locations along the part of floor travelled by the AGV

5.4 Possible sources of errors of the proposed method

This study intends to develop a simplified numerical model which includes a reduced sub-structural floor system and vehicle moving force spectra for various weights and speeds, to evaluate the AGV-induced floor vibrations in LCD factories. The continuous floor systems with thicker RC slabs supported by long-span truss-type steel frames are composite structures and more complicated as compared to pure RC floors. If the dynamic characteristics of the proposed sub-structural floor system travelled by AGVs do not represent those of the original long-span floor system, errors in the floor vibration level would be induced when performing the dynamic

numerical simulation. In order to obtain the realistic floor vibration frequencies of the target LCD factory, this study conducted in-situ floor micro-vibration measurements, from which the equivalent flexural rigidity of the reduced composite floor system was adjusted accordingly. If the experimental results are not available, one may obtain the structural parameters of the equivalent sub-structural floor system from the finite element model (ETABS or SAP2000) that is normally constructed during the design stage of LCD buildings. Moreover, the reduced sub-structural floor system developed in this study is only for one specific line of AGV. However, there may be several lines of AGV (or RGV and stocker) travelling on the whole production floors in LCD factories. If the distance between two lines (at different bays) of AGV is too close, the vibration level would not be predicted well by the proposed method because the vibration interference would exist between each other. Finally, the AGV moving force patterns (intensity and bandwidth) for various weights and speeds simulated by the proposed regressional MKT PSD functions experimentally obtained in the laboratory, may not fully represent those AGVs used in LCD factories because various types of AGVs with different suspension and driving (motor) systems are designed. Despite of this, if the intensity and predominated frequency bandwidth parameters of the PSD functions for specific AGVs could be properly adopted, the comparable simulated floor vibration levels for LCD factories can be achieved.

6. Conclusions

This study explored the AGV-induced vertical micro-vibrations on long-span floors of LCD manufacturing factories. A reduced sub-structural multiple-span continuous beam model that considers only the part of floor travelled by the AGV without constructing a finite element model of the entire storey was adopted to efficiently assess the AGV-induced floor micro-vibrations. The AGV moving loads (or engine forces) corresponding to various AGV weights and speeds were simulated by a proposed regressional modified Kanai-Tajimi power spectral density function that was developed by conducting a series of vehicle-induced vibration tests of a small-scale three-span continuous steel beam model in the laboratory. The dynamic floor responses induced by AGVs with different static weights and moving speeds were resolved using a state-space procedure algorithm. In accordance with the results obtained from experimental tests and numerical simulations, the following conclusions may be drawn.

1. The numerical responses of the small-scale three-span continuous steel beam model simulated by using the first four vibration modes and the identified moving force time histories are shown to correspond well with the experimental dynamic responses obtained in this study. The maximum global error index (GEI) between the experimental and numerical RMS acceleration spectra at the central location of the middle span is 13.07%. This indicates that the dynamic vehicle moving force (or engine force induced by a motor) time histories identified by using the experimentally monitored acceleration time histories are reliable.
2. The best-fitting parameters that govern the modified Kanai-Tajimi moving force power spectral density functions under various vehicle static weights and moving speeds can be obtained through a regression analysis by using the identified one-third octave band moving force spectra. Hence, the moving force pattern (intensity and bandwidth) corresponding to specific vehicle weight and moving speed can be determined by using the regressional modified Kanai-Tajimi moving force power spectral density function as developed in this study.
3. The AGV moving forces of various AGV weights and moving speeds are simulated by the

proposed regressional Kanai-Tajimi model considering the upper-bounded frequency of the predominated moving force bandwidth as 50 Hz and the maximum moving force as 2943 N. The simulation results indicate that the maximum vertical floor micro-vibrations of the target LCD factory may fall within the VC-B and VC-C levels when AGV moves at a lower speed of 1.0 m/s, while they may exceed the VC-B level as required for the installation of most vibration-sensitive tools, when AGV moves at a higher speed of 1.5 m/s. The simulated results of the target LCD factory are comparable to the measured micro-vibration levels of typical LCD factories induced by AGVs moving normally at a speed between 1.0 m/s and 2.0 m/s. Therefore, the AGV-induced floor micro-vibrations predicted by the simplified sub-structural multi-span continuous beam model, together with the AGV engine forces simulated by the proposed regressional modified Kanai-Tajimi moving force model, are considered adequate and reliable for the practical engineering application in LCD factories.

4. The regressional Kanai-Tajimi PSD function for various vehicle weights and speeds directly identified from the experimental vibration history data of the three-span continuous steel beam model used in this study may include the surface irregularity effect; however, this condition may not be the case as in the LCD factory. Despite of the fact that the RC slab (or the alloyed raised floor) irregularities of the production areas in high-tech factories are less significant than those of blacktop roads and traditional factories, this study suggests taking various slab flatness conditions into account to evaluate the roughness effect on the AGV-induced floor vibration level.

Acknowledgements

The research described here was supported by the Research Grants Council of the Hong Kong SAR (Project No. HKU7166/08E) and The University of Hong Kong (Small Project Funding, Project Code: 201007176174). Moreover, the authors thank Dr. Tony Si and Mr. Zhenhu Li, Department of Civil Engineering, The University of Hong Kong, for sharing their experience of the operation of data acquisition systems.

References

Amick, H. and Bui, S.K. (1991), "A review of several methods for processing vibration data", *Proceedings of International Society for Optical Engineering (SPIE)* **1619**, San Jose, November.

Au, F.T.K., Jiang, R.J. and Cheung, Y.K. (2004), "Parameter identification of vehicles moving on continuous bridges", *J. Sound Vib.*, **269**(1-2), 91-111.

Borse, G.J. (1997), *Numerical Methods with MATLAB: A Resource for Scientists and Engineers*, PWS Publishing, Boston.

Computers and Structures Inc. (2002), *ETABS: Three Dimensional Static and Dynamic Analysis of Structures-A Physical Approach with Emphasis on Earthquake Engineering*, Berkeley, California.

Computers and Structures Inc. (2005), *SAP2000: Static and Dynamic Finite Element Analysis of Structures-User's Manual*, Berkeley, California.

Clough, R.W. and Penzien, J. (1993), *Dynamics of Structures*, McGraw-Hill, New York.

Chan, T.H.T., Law, S.S. and Yung, T.H. (1999), "An interpretive method for moving force identification", *J. Sound Vib.*, **219**(3), 503-524.

Chan, T.H.T., Yu, L. and Law, S.S. (2000), "Comparative studies on moving force identification from bridge strains in laboratory", *J. Sound Vib.*, **235**(1), 87-104.

Chan, T.H.T., Yu, L., Law, S.S. and Yung, T.H. (2001a), "Moving force identification studies, I: theory", *J. Sound Vib.*, **247**(1), 59-76.
Chan, T.H.T., Yu, L. and Law, S.S. (2001b), "Moving force identification studies, II: comparative studies", *J. Sound Vib.*, **247**(1), 77-95.
Chan, T.H.T. and Ashebo, D.B. (2006), "Theoretical study of moving force identification on continuous bridges", *J. Sound Vib.*, **295**(3-5), 870-883.
Deng, L. and Cai, C.S. (2010), "Identification of dynamic vehicular axle loads: theory and simulation", *J. Vib. Control*, **16**(14), 2167-2194.
Deng, L. and Cai, C.S. (2011), "Identification of dynamic vehicular axle loads: demonstration by a field study", *J. Vib. Control*, **17**(2), 183-195.
Gordon, C.G. (1991), "Generic criteria for vibration sensitive equipment. Vibration control in microelectronics", *Proceedings of International Society for Optical Engineering (SPIE)*, **1619**, San Jose, November.
Howard, C.Q. and Hansen, C.H. (2003), "Vibration analysis of waffle floors", *Comput. Struct.*, **81**(1), 15-26.
Jiang, R.J., Au, F.T.K. and Cheung, Y.K. (2003), "Identification of masses moving on multi-span beams based on a genetic algorithm", *Comput. Struct.*, **81**(22-23), 2137-2148.
Jang, Y.J. and Choi, G.H. (2006), "Introduction to automated material handling systems in LCD panel production lines", *Proceeding of the 2006 IEEE, International Conference on Automation Science and Engineering*, Shanghai, October.
Ju, S.H. (2009), "Finite element investigation of traffic induced vibrations", *J. Sound Vib.*, **321**(3-5), 837-853.
Lee, C.L., Wang, Y.P. and Su, R.K.L. (2012a), "A study on AGV-induced floor micro-vibration in TFT-LCD high technology fabs", *Struct. Control Hlth.*, **19**(3), 451-471.
Lee, C.L., Wang, Y.P. and Su, R.K.L. (2012b), "Assessment of vibrations induced in factories by automated guided vehicles", *P. I. Civil Eng.-Struct. Build.* (Accepted).
Law, S.S., Chan, T.H.T. and Zeng, Q.H. (1997), "Moving force identification: a time domain method", *J. Sound Vib.*, **201**(1), 1-22.
Law, S.S., Chan, T.H.T. and Zeng, Q.H. (1999), "Moving force identification-a frequency and time domains analysis", *J. Dyn. Syst.-T. ASME*, **121**(3), 394-401.
Law, S.S., Bu, J.Q., Zhu, X.Q. and Chan, S.L. (2007), "Moving load identification on simply supported orthotropic plate", *Int. J. Mech. Sci.*, **49**(11), 1262-1275.
Law, S.S. and Zhu, X.Q. (2011), *Moving Loads: Dynamic Analysis and Identification Techniques*, CRC Press, Boca Raton, Florida.
Lopez-Almansa, F., Harbat, A.H. and Rodellar, J. (1988), "SSP algorithm for linear and nonlinear dynamic response simulation", *Int. J. Num. Meth. Eng.*, **26**(12), 2687-2706.
Nguyen, T.H., Gad, E.F., Wilson, J.L. Haritos, N. (2012), "Improving a current method for predicting walking-induced floor vibration", *Steel Compos. Struct*., **15**(2), 139-155.
Pan, T.C., Mita, A. and Li, L. (2001), "Vehicle-induced floor vibration in a multistory factory building", *J. Perform. Constr. Facil. (ASCE)*, **13**(2), 54-61.
Pavic, A. and Reynolds, P. (2002), "Vibration serviceability of long-span concrete building floors: part 1– review of background information", *Shock Vib. Dig.*, **34**(3), 191-211.
Pavic, A. and Reynolds, P. (2003), "Evaluation of mathematical models for predicting walking-induced vibrations of high-frequency", *Int. J. Struct. Stab. Dyn.*, **3**(1), 107-130.
Pan, T.C., Mita, A. and Li, L. (2008), "Evaluation of floor vibration in a biotechnology laboratory caused by human walking", *J. Perform. Constr. Facil. (ASCE)*, **22**(3), 122-130.
Shinozuka, M. (1971), "Simulation of multivariate and multidimensional random processes", *J. Acoust. Soc. Am.*, **49**(1), 357–368.
Tang, N., Amick, H. and Gendreau, M. (2009), "Long-span truss structures for low-vibration environments", *Proceedings of ASCE/SEI Structures 2009 Congress*, Austin Texas, April.
Ungar, E.E. and White, R.W. (1979), "Footfall-induced vibrations of floors supporting sensitive equipment", *Sound Vib.*, **13**(10), 10-13.

Ungar, E.E., Zapfe, J.A. and Kemp, J.D. (2004), "Predicting footfall-induced vibration of floors", *Sound Vib.*, **38**(11), 16-22.
Wang, Y.P., Lee, C.L. and Yo, T.H. (2001), "Modified state-space procedures for pseudodynamic testing", *Earthq. Eng. Struct. D.*, **30**(1), 59-80.
Wang, Y.P., Liao, W.H. and Lee, C.L. (2003), "Seismic risk of typical double fabs in Taiwan's Hi-Tech industry", *Proceedings of the Joint NCREE/JRC Workshop International Collaboration on Earthquake Disaster Mitigation Research*, Taiwan, November.
Willford, M., Young, P. and Field, C. (2005), "Improved methodologies for the prediction of footfall-induced vibration", *Proceedings of International Society for Optical Engineering (SPIE)* **5933**, San Diego, July.
Xu, Y.L., Guo, A.X., Li, H. and Ng, C.L. (2004), "Hybrid control of microvibration of high tech facility under horizontal and vertical ground", *Proceedings of International Society for Optical Engineering (SPIE),* **5391**, San Diego, March.
Xu, Y.L. and Guo, A.X. (2006), "Microvibration control of coupled high tech equipment-building systems in vertical direction", *Int. J. Solids Struct.*, **43**(21), 6521-6534.
Xu, Y.L. and Hong, X.J. (2008), "Stochastic modelling of traffic-induced building vibration", *J. Sound Vib.*, **313**(1-2), 149-170.
Yang, J.N. and Agrawal, A.K. (2000), "Protective systems for high-technology facilities against microvibration and earthquake", *Struct. Eng. Mech.*, **10**(6), 561-575.
Yu, L. and Chan, T.H.T. (2003), "Moving force identification based on the frequency-time domain method", *J. Sound Vib.*, **261**(2), 329-349.
Yu, L. and Chan, T.H.T. (2007), "Recent research on identification of moving loads on bridges", *J. Sound Vib.*, **305**(1-2), 3-21.
Zheng, D.Y., Cheung, Y.K., Au, F.T.K. and Cheng, Y.S. (1998), "Vibration of multi-span non-uniform beams under moving loads by using modified beam vibration functions", *J. Sound Vib.*, **212**(3), 455-67.
Zhu, X.Q. and Law, S.S. (2002), "Practical aspects in moving load identification", *J. Sound Vib.*, **258**(1), 123-146.
Živanović, S. and Pavić, A. (2009), "Probabilistic modeling of walking excitation for building floors", *J. Perform. Constr. Facil. (ASCE)*, **23**(3), 132-143.